

Spectroscopy of nonlinear band structures of one-dimensional photonic crystals

Christian E. Rüter and Detlef Kip*

Institute of Physics and Physical Technology, Clausthal University of Technology, 38678 Clausthal-Zellerfeld, Germany

(Received 20 August 2007; revised manuscript received 25 October 2007; published 18 January 2008)

The temporal development of extended nonlinear modes of a one-dimensional photonic crystal during the build-up of the nonlinearity is experimentally investigated. For this a prism coupling setup is used, which allows for a direct comparison of linear and nonlinear photonic band structures. The experimental results are compared with numerical calculations which make use of the Floquet-Bloch approach and the finite difference approximation.

DOI: [10.1103/PhysRevA.77.013818](https://doi.org/10.1103/PhysRevA.77.013818)

PACS number(s): 42.70.Qs, 42.40.Ht, 42.65.Tg

I. INTRODUCTION

Periodic photonic structures have been studied extensively both theoretically and experimentally over the last decades, see, e.g., Ref. [1]. Due to the spatially periodic refractive index distribution wave propagation in such systems differs fundamentally from that in homogeneous optical media, but at the same time it exhibits characteristics known from other periodic systems such as semiconductor lattices, molecular chains, or coupled pendular. The linear modes of periodic photonic structures are extended Floquet-Bloch (FB) modes. Their longitudinal propagation constants depend strongly on the transverse wave vector component and form a transmission spectrum consisting of allowed bands and forbidden gaps. This transmission spectrum defines the propagation direction and the diffraction characteristics of an incident optical beam.

Waveguide arrays are one-dimensional (1D) realizations of periodic photonic structures. The first experiments revealing the properties of discrete diffraction in such systems were made using III-V semiconductors [2]. The same type of arrays of coupled channel waveguides was also used to demonstrate that the presence of a nonlinear medium can alter the diffraction characteristics and lead to the formation of localized states, so-called discrete solitons [3], as predicted by Christodoulides *et al.* [4]. These experiments initiated a series of studies revealing more linear properties of periodic photonic structures including the observation of anomalous diffraction [5], realization of diffraction management [6], and the measurement of transmission spectra (band structures) and intensity distributions of FB modes [7]. By using highly nonlinear materials, for example photorefractive crystals, localized nonlinear structures [8–11], Bloch oscillations [12], and modulational instabilities [13–15] were discovered.

In a previous publication we demonstrated that a prism coupler can be used to determine the linear band structures of 1D waveguide arrays [16]. In this contribution we show that the same technique can also be utilized to examine the nonlinear index changes altering the propagation constants of extended FB modes, which enables time-resolved measurements of nonlinear band structures and forms the base for future experiments on Zener tunneling, multiband mixing,

and vector soliton formation. This work is organized as follows. First we give a short description of the experimental procedure and the sample used. After this, experimental results for extended modes of all guided bands of the sample are presented. This includes measured changes in the propagation constants of the excited FB modes itself as well as the influence of these induced nonlinear refractive index changes on the whole band structure. Finally a simple theoretical model will be presented to discuss the experimental results obtained.

II. EXPERIMENTAL METHODS

For the experiments a prism coupling setup in a retro reflective scheme and green light of an Ar⁺ laser (wavelength $\lambda=514.5$ nm) is used. Light coupled into the high-index prism is totally reflected at the interface of prism base and sample. By varying the angle of incidence the wave vector component parallel to the prism base can be controlled. If this component matches the propagation constant of a mode of the sample light couples into this mode due to optical tunneling. The intensity reflected at the prism base as a function of the angle of incidence forms a mode spectrum of the sample. As stated in Ref. [16] the transverse wave vector component, the Bloch momentum k_z , can be adjusted by tilting the waveguide array relative to the plane of incidence. A series of mode spectra for different tilt angles gives the longitudinal propagation constants of the guided FB modes as a function of k_z . This is the band structure of the sample. Instead of the propagation constant β the effective refractive index $n_{\text{eff}}=\beta/k_0=\beta\lambda/2\pi$ is used here. The waveguide array is fabricated in Fe-doped *x*-cut LiNbO₃ (LN) using Ti in-diffusion [17]. Iron increases the impurity level and thus increases the photorefractive effect in LN. The waveguide array which possesses a saturable defocusing nonlinearity [18] consists of 250 channels with a width of 5 μm and has a grating period of $\Lambda=8$ μm . The array was prepared by patterning a 5 nm thick Ti layer. Before in-diffusion for 2 h at 1273 K a second homogeneous layer with a thickness of 5 nm was deposited on top of the patterned stripes. The 22 mm long channels run parallel to the *y* axis and the grating vector is parallel to the crystallographic *c* axis of the crystal [16].

The experimental procedure to measure nonlinear changes induced by the intensity distribution of a certain excited FB

*d.kip@pe.tu-clausthal.de

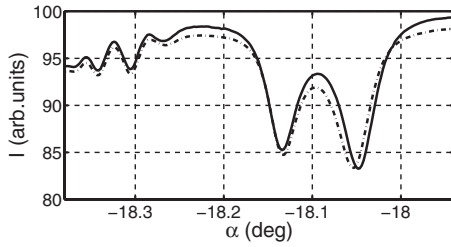


FIG. 1. Measured reflected light intensity I versus incident angle α at $k_z = \pi/\Lambda$, before (solid line) and after (dashed line) a mode of the first band was excited for 200 min with $P_{\text{in}} \approx 0.11 \mu\text{W}$ per channel.

mode is as follows. First, before any nonlinear measurements, the full linear band structure is measured. Here a low light intensity is used for the incident beam such that the power coupled into the waveguide array does not exceed $10^{-3} \mu\text{W}$ per channel. After the linear band structure has been measured, the angle α , being the angle formed between the incident laser beam and the normal-to-the-input face of the prism, is adjusted to excite the FB mode of interest with fixed value of k_z . Then the input intensity of this mode is increased. Due to the nonlinear refractive index changes induced by the intensity distribution of the FB mode and thermal effects discussed below the angle α has to be readjusted to fulfill the transverse phase matching condition. During the nonlinear excitation a mode spectrum with fixed k_z is measured every five minutes. From these mode spectra the propagation constants of the guided modes and substrate radiation modes are determined. In this way the influence on the other FB modes at the selected value of k_z used can be studied. At the end of the experiment the input intensity is reduced, and the complete band structure for all k_z is measured again. Finally, before restarting a new measurement, all induced nonlinear refractive index changes are erased using white light illumination.

The example given in Fig. 1 shows a linear (solid line) and a nonlinear (dashed line) mode spectrum at the edge of the Brillouin zone (BZ) at $k_z = \pi/\Lambda$. In this experiment the mode of the first band has been excited for 200 min with an in-coupled power of $P_{\text{in}} \approx 0.11 \mu\text{W}$ per channel. A clear change of the mode spectrum can be seen. As higher values of the angle α correspond to higher values of refractive index the effective refractive index n_{eff} of the mode of the first band has been reduced in the nonlinear case. The coupling angle of the mode of the second band has been slightly shifted to higher values, i.e., the effective refractive index is increased. The mode of the third band is not visible in this spectrum because this mode is both, weakly guided for $k_z = \pi/\Lambda$ and hardly excited because of the quite small overlap with the plane wave entering the prism.

As can be seen in Fig. 1 the coupling angle corresponding to the refractive index of the substrate is hard to determine. There is no sharp bend and the typical decay of the reflected intensity for coupling angles corresponding to effective refractive indices smaller than the substrate index is superimposed with several minima [19]. These minima correspond to intensity distributions localized below the waveguide array

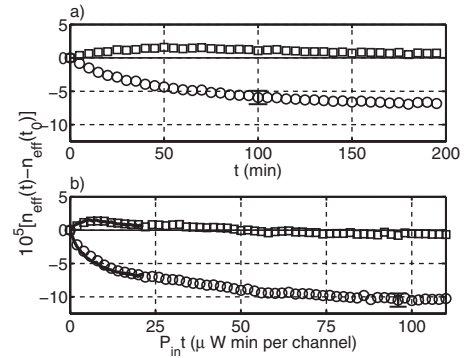


FIG. 2. (a) Effective refractive index changes of the modes of the first (circles) and second (squares) band versus time when a mode of the first band at $k_z = \pi/\Lambda$ is excited with $P_{\text{in}} \approx 0.11 \mu\text{W}$ per channel. (b) Measurement as shown in (a) (solid lines) and for $P_{\text{in}} \approx 0.4 \mu\text{W}$ per channel.

having only a very small fraction of their intensity distribution in the region of the waveguides. It can be expected that these substrate radiation modes are only very weakly affected by the nonlinear changes of the waveguide array. Therefore, their coupling angles can be used as reference points. In addition to the changes of the effective refractive index of the guided modes a shift of the whole mode spectrum is observed in the experiments. This shift is of the order of 0.01° to 0.04° and always positive. No correlation between the magnitude of the shift and the intensity of the in-coupled light could be found, but the time dependent behavior indicates that thermal effects are responsible for this effect. The high thermal sensitivity of prism coupling setups has already been described by Holman *et al.* [20], which is due to the temperature dependence of the refractive index of LN and the rutile prism used. With the thermo-optic coefficients for the extraordinary refractive indices of LN [21] and rutile [22] it is found that a temperature change of 3 K induces a shift of 0.04° of the coupling angle. As this temperature change increases the extraordinary refractive index of LN by 5×10^{-5} and decreases the extraordinary refractive index of rutile by 4×10^{-4} the observed shift of the mode spectra can be mainly attributed to index changes of the prism. Furthermore the thermal influence on the band structure, meaning the difference between effective refractive indices of the modes and the substrate index, may be neglected because $\Delta n_{\text{eff}}/\Delta T \approx \Delta n_e/\Delta T$ can be assumed [23].

III. EXPERIMENTAL RESULTS

The influence of the nonlinear refractive index changes induced by the intensity distribution of an excited FB mode on the mode itself and the whole band structure is analyzed using the procedure described above. For this FB modes of all three guided bands at different points of the BZ are used.

In Fig. 1 the linear and nonlinear mode spectra for the excitation of the FB mode of the first band at $k_z = \pi/\Lambda$ were given. The corresponding temporal evolution of the effective refractive index changes of the two FB modes located in the first and second band is given in Fig. 2(a). The effective

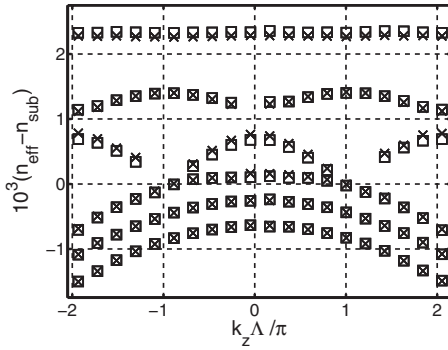


FIG. 3. Measured band structure before (squares) and after (crosses) the mode of the first band had been excited at $k_z = \pi/\Lambda$ for 200 min with $P_{in} \approx 0.11 \mu\text{W}$ per channel.

index of the first mode (circles) decreases while in the second band (squares) the mode's effective index increases first but decreases after reaching a maximum value. Figure 2(b) shows the results of a second experiment with a higher in-coupled power and longer excitation time. Here changes are not given as a function of time but as a function of energy. As it is known from two-beam interference experiments in Fe-doped LN, the maximal value of the nonlinear refractive index change does not depend on light intensity, provided that the dark intensity is negligible and that the time constant is inversely proportional to light intensity. This means increasing the intensity will only speed up the process and index changes obtained for different intensities coincide if plotted as a function of energy. The data from part (a) is given as solid lines in Fig. 2(b). The curves agree well within the margin of error, which is approximately $\pm 2 \times 10^{-5}$ in these experiments. As can be seen the changes for the mode of the first band saturate and the mode's effective refractive index is reduced by 10^{-4} . The mode of the second band increases first and afterwards decreases to a value slightly smaller than in the linear case.

Figure 3 shows the nonlinear band structure (crosses) measured at the end of the experiment given in Fig. 2(a). For comparison the linear case (squares) before illumination is shown, too. The uncertainty in these measurements is approximately $\pm 5 \times 10^{-5}$, which is mainly due to the error in the adjustment of k_z . To improve the accuracy the band structure measurements are performed covering two full BZ's. It turns out that the effective refractive index of the first band is reduced throughout the BZ. The second band is almost unshifted, but small changes in the vicinity of the center of the BZ (data for $|k_z| = 0.2\pi/\Lambda$) indicate that the curvature of the band has increased. Similar conclusions can be also drawn for the diffraction of the third band in the BZ center. At the same time the effective refractive indices of modes of the third band are shifted towards higher values. Thus the gaps between all neighboring bands are reduced.

To examine if the changes induced by modes of the first band depend on Bloch momentum experiments were repeated for excitations at several other points of the BZ. It turns out that the nonlinear band structures corresponding to these experiments are very similar to the result obtained for $k_z = \pi/\Lambda$. The effective refractive index changes are compa-

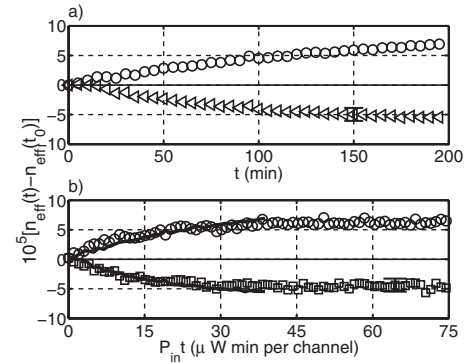


FIG. 4. (a) Effective refractive index changes of modes of first band (circles) and second band (squares) versus time for excitation of the second band at $k_z = \pi/\Lambda$ with $P_{in} \approx 0.19 \mu\text{W}$ per channel. (b) Data from (a) (solid lines) and for a second measurement with $P_{in} \approx 0.2 \mu\text{W}$ per channel.

table for all modes located in the first band. On the other hand, the changes of the modes lying in the second and third band depend on k_z , as indicated by the nonlinear band structure.

Next we move over to excitation of modes of the second band, starting at the edge of the BZ. Figures 4(a) and 4(b) show the temporal behavior of the effective refractive index changes for the modes of the first (circles) and second (squares) band. In saturation the effective refractive index of the mode lying in the second band is reduced by 5×10^{-4} whereas in the first band the index is increased by a slightly higher value.

The linear (squares) and nonlinear (crosses) band structures corresponding to the experiment in Fig. 4(a) are given in Fig. 5. Changes in the first and second band are nearly constant throughout the BZ. The first band is shifted to higher values whereas the second band is shifted towards smaller values. The third band remains constant. No clear conclusions can be drawn on changes of diffraction coefficients from this measurement.

When a mode of the second band is excited in the center of the BZ at $k_z = 2\pi/\Lambda \equiv 0$ a significantly different band structure is obtained when compared with the experiment for $k_z = \pi/\Lambda$, see Fig. 6. This is different to the excitations using

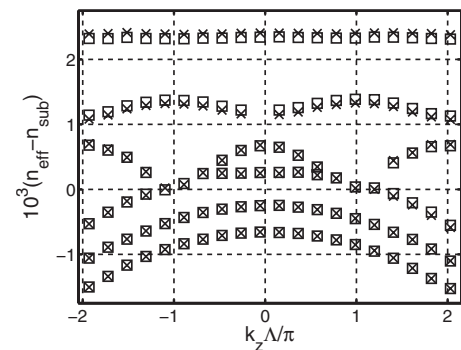


FIG. 5. Measured band structure before (squares) and after (crosses) the second band had been excited at $k_z = \pi/\Lambda$ for 200 min with $P_{in} \approx 0.19 \mu\text{W}$ per channel.

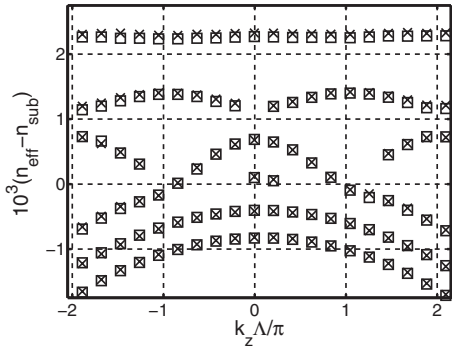


FIG. 6. Measured band structure before (squares) and after (crosses) the mode of the second band had been excited at $k_z=2\pi/\Lambda$ for 360 min with $P_{in} \approx 0.35 \mu\text{W}$ per channel.

modes of the first band presented before. The induced nonlinear index changes shift the first band towards higher values. While the second band itself remains mostly unshifted, the curvature of this band is reduced in the center, accompanied by a small increase of the effective refractive indices of the corresponding modes. The latter can be also observed in the temporal evolution of the light-induced changes in Figs. 7(a) and 7(b). Here effective refractive index changes for modes of the first (circles), second (squares), and third (triangles) band are given for two different values of the in-coupled power. The band structure in Fig. 6 corresponds to data obtained for $P_{in} \approx 0.35 \mu\text{W}$. The decrease of the effective refractive index of the mode located in band three indicates that the curvature is reduced. Additionally it can be stated that the temporal evolution of the effective refractive index changes shows zero crossings for modes of the second and third band, while for modes in band one a monotonic increase is found. These results show that the changes in the band structures induced by the modes of the second band depend strongly on the value of k_z . Measurements at intermediate points indicate that these changes change continuously from the center of the BZ to the edge.

As already stated modes of the third band are hardly guided at $k_z=\pi/\Lambda$. Therefore only results obtained for mode

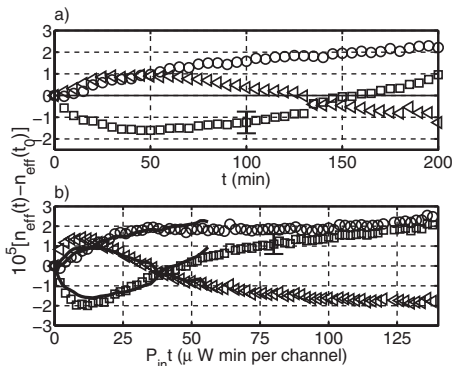


FIG. 7. (a) Measured effective index changes for the modes of the first (circles), second (squares), and third (triangles) band versus time for excitation of the FB mode of the second band at $k_z=2\pi/\Lambda$ with $P_{in} \approx 0.2 \mu\text{W}$ per channel. (b) Measurement as shown in (a) (solid lines) and for $P_{in} \approx 0.35 \mu\text{W}$ per channel and longer excitation time over $P_{in}t$.

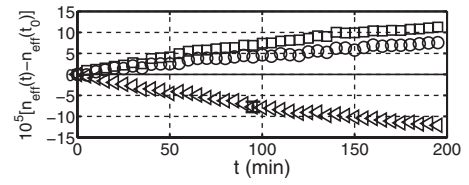


FIG. 8. Measured change of the effective refractive of the mode of the first (circles), second (squares), and third (triangles) band versus time for excitation of the FB mode of the third band at $k_z=2\pi/\Lambda$ with $P_{in} \approx 0.25 \mu\text{W}$ per channel.

excitation in the third band at $k_z=2\pi/\Lambda$ can be presented. In Fig. 8 it can be observed that the nonlinear changes of the refractive index induced by the intensity distribution of the third band influence all three guided bands. The effective refractive index of modes located in the first (circles) and second (squares) band are increased by 10^{-4} , while values in the excited third band (triangles) are reduced by the same amount. When comparing the corresponding linear (squares) and nonlinear (crosses) band structures in Fig. 9 the same holds true for the bands as a whole.

IV. MODELING

In this section a rather simple theoretical model for the calculation of band structures of nonlinear waveguide arrays will be presented. First the refractive index profile of the waveguide array is calculated by solving the diffusion equation for a depletable source using parameters related to the experimental data given above. The resulting Ti concentration profile is transferred into a refractive index distribution using the method described in Ref. [24]. We start with the scalar Helmholtz equation for TE polarized modes propagating in the y direction,

$$[-\partial_x^2 + \beta^2 - k_0^2 \epsilon_3(x, z) - \partial_z \epsilon_2^{-1}(x, z) \partial_z \epsilon_3(x, z)] E_3(x, z) = 0. \quad (1)$$

The calculated refractive index profile enters Eq. (1) in the diagonal elements of the second rank permittivity tensor $\epsilon_i(x, z) = n_i^2(x, z)$. The only nonzero element of the electric

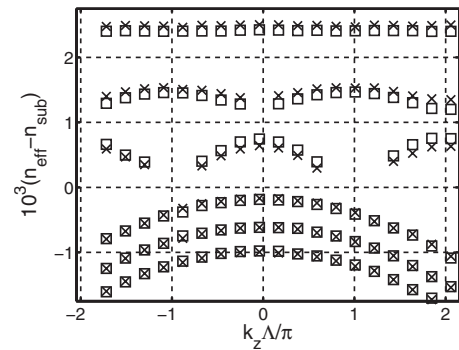


FIG. 9. Measured band-gap structure before (squares) and after (crosses) the mode of the third band had been excited at $k_z=2\pi/\Lambda$ for 200 min with $P_{in} \approx 0.25 \mu\text{W}$ per channel.

field vector is the z component $E_3(x, z)$. Assuming a weakly guiding structure with a slowly varying refractive index profile the equation can be further simplified:

$$\{-\partial_x^2 + k_0^2[n_{\text{eff}}^2 - \varepsilon_3(x, z)] - (n_o/n_e)^2\partial_z^2\}E_3(x, z) = 0. \quad (2)$$

In the case of a single isolated channel waveguide this equation can be solved using the finite difference approach. Here this approach is used for the x direction only. As the refractive index changes induced by Ti in-diffusion decay exponentially along x it can be expected that the component $E_3(x, z)$ will also show a strong dependency on x . In the z direction the refractive index profile is spatially periodic with grating period Λ . Using the Bloch ansatz the solution is supposed to be of the form $E_3(x, z) = E(x, z)\exp(-1k_z z)$, with the periodic function $E(x, z) = E(x, z + \Lambda)$ and Bloch momentum k_z . The periodic function $E(x, z)$ is written as a Fourier series

$$E(x, z) = \sum_{m=-\infty}^{\infty} a_m(x)\exp(1mKz), \quad (3)$$

with grating vector $K = 2\pi/\Lambda$. Using a constant grid in the x direction the periodic function can be expressed as follows:

$$E(x, z) = \sum_{n=0}^N \sum_{m=-\infty}^{\infty} a_{m,n} \exp(1mKz). \quad (4)$$

The permittivity is written in an analogous way with the amplitudes $\varepsilon_{m,n}$.

With these assumptions, Eq. (2) is transferred into an eigenvalue equation for the effective refractive index n_{eff} and the electric field amplitudes $a_{m,n}$ as a function of k_z :

$$\begin{aligned} & -\frac{a_{m,n+1} - 2a_{m,n} + a_{m,n-1}}{\Delta x^2} \\ & + [k_0^2(n_{\text{eff}}^2 - \varepsilon_{m,n}) - (n_o/n_e)^2(-m^2K^2 + 2mk_zK - k_z^2)]a_{m,n} \\ & = 0. \end{aligned} \quad (5)$$

The effective refractive indices obtained describe the band structure of the array when plotted over k_z . From the amplitudes of the electric field the intensity distributions of the FB modes can be calculated, showing good agreement with experimental results, see Ref. [16] for further details.

In the nonlinear case the intensity distributions will induce nonlinear refractive index changes via the photorefractive effect. The response of Fe-doped photorefractive LN to inhomogeneous illumination is described by the one-center band-transport model [25]. In this model the photorefractive effect is due to photoionization, redistribution of excited charge carriers and their retrapping at different locations, which finally results in the build-up of space-charge fields altering the refractive index via the electro-optic effect. The corresponding nonlinear rate equations have been intensively studied for the case of two-beam interference experiments, see Ref. [26], and references therein. Analytical solutions have been found for single gratings with sinusoidal intensity distribution and small modulation depths [25]. In that case only the first harmonic of the space-charge field has to be considered. However, for large modulation depths and superimposed or sequentially recorded gratings, substantial contri-

butions of higher harmonics were observed experimentally and predicted theoretically, see, e.g., Refs. [27–32], including sum and difference grating formation. The present problem can be understood as a special case of holographic recording of superimposed gratings. The intensity distribution of a FB mode cannot be described by a single sinusoidal function. It has to be expanded in a Fourier series of the grating vector K , including higher harmonics. All these gratings are recorded simultaneously and influence each other leading to a rather strong interaction.

For the following simulations the rate equations given in Ref. [25] are further simplified. First, as in the band structure calculations, the crystal is discretized in the x direction. Each layer is assumed to be independent from the others, thus neglecting diffusion of excited charge carriers as well as space-charge fields along the x direction. In this way the scalar equations used to describe two-beam interference experiments are applicable. The one-center band-transport model in LN is described by

$$-\partial_z j(z) = \epsilon_0 \epsilon_{33} \partial_z E_{\text{SC}}(z), \quad (6)$$

$$j(z) = e\mu\tilde{n}_e(z)E_{\text{SC}}(z) + \beta_{33}I(z), \quad (7)$$

$$0 = \gamma(I(z) + I_D) - \frac{1}{\tau}\tilde{n}_e(z) + \frac{1}{e}\partial_z j(z), \quad (8)$$

with permittivity ϵ_{33} , space-charge field $E_{\text{SC}}(z)$, and current density $j(z)$. As the periodic refractive index modulation of the array is small, ϵ_{33} is assumed to be constant in Eq. (6). The bulk photovoltaic effect dominates the charge transport, thus we neglected diffusion terms in Eq. (7). Here we used the Glass notation [33], with intensity $I(z)$ and the corresponding tensor element β_{33} for the bulk photovoltaic effect. The remaining quantities are the mobility of the excited electrons μ and the electron density in the conduction band $\tilde{n}_e(z)$. In Eqs. (8) the time derivative of $\tilde{n}_e(z)$ is neglected: as the electron trapping rate in LN exceeds any other rate by several orders of magnitude, the electrons reach the local equilibrium almost instantaneously [34]. Additionally, the density of filled and empty traps is assumed to be constant throughout the sample. Therefore the generation constant γ and the recombination time constant τ are introduced. The dark intensity I_D accounts for thermal generation of electrons. For each layer the intensity distribution is of the form

$$I(z) = \sum_{m=-N}^N I_m \exp(1mKz),$$

with $I_{-m} = I_m$. The current density, electron density, and space-charge field are expressed in terms of the grating vector K , too.

From Eqs. (8) and (7) expressions for the amplitudes of the electron density are obtained:

$$\tilde{n}_0 = \gamma\tau(I_0 + I_D), \quad a_m = \frac{I_m\gamma\tau}{\tilde{n}_0} = \frac{I_m}{I_0 + I_D},$$

where \tilde{n}_0 is the constant part and a_m are the amplitudes of higher harmonics m . Here we assume that the electron den-

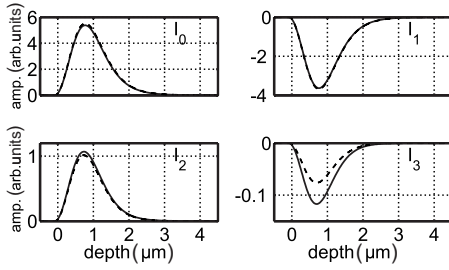


FIG. 10. Amplitudes of the constant component and the first three spatial harmonics of the intensity distribution forming the mode of the first band at $k_z = \pi/\Lambda$ over the crystal depth. The solid and dashed lines represent the amplitudes in the linear and nonlinear case, respectively.

sity is unshifted with respect to the intensity distribution [35], and that nonlinear mixing of spatial harmonics can be neglected, as it has been shown numerically by Buchhave [36]. The temporal evolution of spatial harmonics of the space-charge field results from Eqs. (6) and (7):

$$\partial_t E_{SC,m} = -\frac{e\mu\tilde{n}_0}{\epsilon_{33}\epsilon_0} \left(\frac{\beta_{33}}{e\mu\tilde{n}_0} I_m + E_{SC,m} + \sum_{j,k=m}^{j,k \neq 0} a_j E_{SC,k} \right). \quad (9)$$

The boundary condition of a short-circuited sample was used here. Neglecting the mixing term, this equation has the well known analytical solution

$$E_{SC,m} = A_m [1 - \exp(-t/\tau_0)], \quad (10)$$

with $A_m \propto I_m / (I_0 + I_D)$ and $\tau_0 = e\mu\tilde{n}_0 / (\epsilon_{33}\epsilon_0)$.

The assumption of independent spatial harmonics is not valid here, as the higher harmonics have amplitudes comparable to the amplitude of the fundamental grating. Therefore the mutual influence of the spatial harmonics can be expected to play an important role [30]. For this reason Eq. (9) is solved numerically. Starting with the linear intensity distribution of a certain FB mode, the amplitudes of the space-charge field are calculated for a small time step $\Delta t \ll \tau_0$. The corresponding amplitudes of the nonlinear refractive index changes are obtained using $\Delta n_m^{nl} = -0.5n_e^3 r_{33} E_{SC,m}$, with the electro-optic coefficient r_{33} and n_e being the extraordinary refractive index of LN. With this altered index modulation of the lattice the band structure is recalculated, giving new values for the effective refractive index of the FB modes and the amplitudes of the intensity distribution. The old values of the amplitudes of the space-charge field and the new values for the intensity distribution are then used to calculate a new set of space-charge field amplitudes for the next time step Δt . This procedure is repeated until the saturation regime is reached. In all calculations a normalized peak power of 15 for the intensity distribution of the excited FB mode is used. The dark intensity is set to $I_D = 0.1$ and the maximal value of the induced nonlinear refractive index change is set to $\Delta n_{\max}^{nl} = 1.25 \times 10^{-4}$.

We again start our analysis for modes located in the first band at the edge of the BZ. Figure 10 shows the linear amplitudes of the constant component and the first three spatial harmonics forming the intensity distribution of a mode in

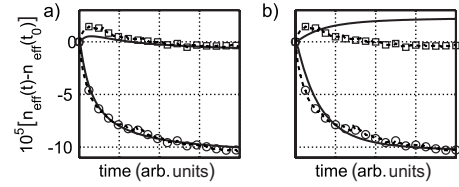


FIG. 11. Comparison of experimental (symbols, dashed lines) and theoretical data (solid lines) using the data from Fig. 2. Theoretical results were obtained with (a) and without (b) the mixing term in Eq. (9).

band one at $k_z = \pi/\Lambda$ as a function of the crystal depth. The dashed line corresponds to the amplitudes obtained by numerically solving Eq. (9). Notice that the nonlinear amplitude changes are small when compared to the linear case. Additionally, the first two spatial harmonics have comparable amplitudes whereas the third and higher harmonics (not shown here) contribute only to a minor degree.

Figure 11 shows the simulated temporal build-up of the effective refractive index changes. For comparison, the theoretical results are plotted together with the experimental data. The time scale of the calculated data is adjusted to fit the experimental ones. Notice that the temporal build-up of the effective refractive index changes for both guided modes is reproduced best in Fig. 11(a), which includes the mixing term in Eq. (9). Comparing the experimental data with the theoretical curves in Fig. 11(b), obtained without the mixing term, shows not only clear deviations for the mode located in band two, but also differs in the temporal evolution of the effective refractive index of the mode of the first band.

The strong influence of the nonlinear mixing term in Eq. (9) is also illustrated in Fig. 12. Here the amplitudes of nonlinear index changes and the corresponding nonlinear band structures are given. Without the mixing term [i.e., using Eq. (10)], only the first (circles) and second (squares) spatial harmonics of the nonlinear refractive index change deviate from

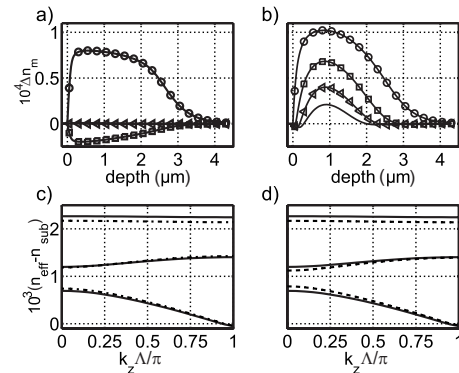


FIG. 12. Nonlinear index changes obtained using the intensity distribution of a mode of the first band at $k_z = \pi/\Lambda$. (a), (b) amplitudes of the spatial harmonics of the nonlinear refractive index changes as a function of the crystal depth. The first (circles), second (squares), third (triangles), and fourth harmonic are shown, both with (a) and without (b) including the nonlinear mixing. (c), (d) Corresponding nonlinear (dashed lines) and linear (solid line) band structure.

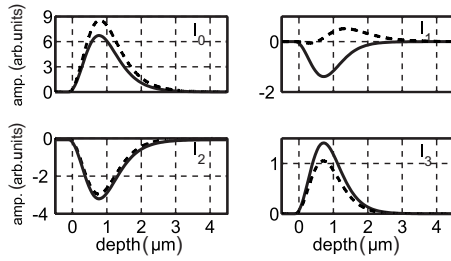


FIG. 13. Modulation of the extraordinary refractive index versus crystal width at the maximum of the intensity distribution of the modes located in the first band. The solid line represents the linear case, while the dashed line corresponds to the profile of the nonlinear band structure from Fig. 12(c). The dotted line shows the intensity distribution.

zero. The nonlinear band structure [dashed line in Fig. 12(c)] shows a decrease of the effective refractive index of the first band and small changes in the second and third band, thus indicating an increase of the curvature of these band when compared with the linear case. On the contrary, when the mixing term is included, higher spatial harmonics of the nonlinear refractive index change appear [Fig. 12(b)]. Additionally, the final amplitudes of the first and second spatial harmonic are markedly influenced. When comparing with the results given in Fig. 12(a) an enhancement of these amplitudes can be recognized. Additionally the sign of the amplitude of the second spatial harmonic has changed. This feedback has been experimentally observed in simultaneous recording of photorefractive gratings in barium titanate crystals, see Ref. [37], and has been theoretically predicted for the same experiments utilizing LN [30]. Comparison of the corresponding linear and nonlinear band structures in Fig. 12(d) shows similar changes as in the experimental section in Fig. 3. The effective refractive index of the first band is reduced throughout the BZ and the diffraction coefficients of the second and third bands are increased. Additionally, all the gaps between neighboring bands are reduced. In the following, only numerical results obtained using the nonlinear mixing term in Eq. (9) will be presented.

The nonlinear band structures obtained for modes located in the first band at different positions of the BZ are quite similar. This means the changes in the effective refractive index for the modes located in the first band are comparable throughout the BZ. As in the experiments the changes differ for modes located in the second and third band and match the values expected by the nonlinear band structure. One reason for this might be that the amplitudes of the spatial harmonics of the intensity distribution for all modes located in the first band deviate only slightly from the values given in Fig. 10.

The effect of the nonlinear refractive index changes induced by the modes of the first band can be understood with regard to Fig. 13. Here the refractive index modulation is given as a function of the crystal width for the layer where the intensity distribution of the modes of the first band is maximal. The solid line corresponds to the linear case, whereas the dashed line refers to the saturation regime of the simulations. The shape of the intensity distribution is included as dotted line. Notice that the maximal value of the

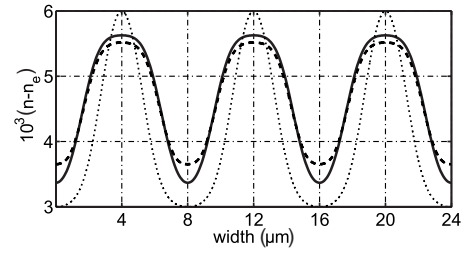


FIG. 14. Amplitudes of the constant component and the first three spatial harmonics of the intensity distribution forming the modes of the second band at $k_z=0$ (solid line) and $k_z=\pi/\Lambda$ (dashed line).

modulation is decreased whereas the refractive index is increased in-between channels. As both, the effective refractive index of the modes located in the first band depends on the maximal value of the modulation, and the size of the gaps on its contrast, this may explain the experimental results.

Next we move over to excitation of modes of band two. The experimental results indicate that in this case the induced index changes depend strongly on the value of the transverse wave vector. In Fig. 14 the amplitudes of the constant part and the first three spatial harmonics contributing to the intensity distribution are plotted for modes located at the center and at the edge of the BZ. One may notice that all amplitudes change distinctively with k_z , indicating that this is one explanation for the experimental observations. Additionally it may be observed that the amplitude of the third harmonic is of the same magnitude as the one of the fundamental harmonic. The fourth and higher harmonics have small amplitudes and are not shown here.

Simulation results for excited modes at the edge of the BZ are plotted in Fig. 15. Generally, the amplitudes of calculated index changes are small when compared to experimental results (see Figs. 4 and 6). Nevertheless a qualitative agreement between theory and experimental curves may be noticed.

Figure 16 illustrates the refractive index changes induced by the intensity distribution of the mode located in the second band at the edge of the BZ. The 1D linear and nonlinear index profiles correspond again to the layer in which the intensity of the mode of the second band is maximal. When comparing the linear and nonlinear profiles it may be ob-

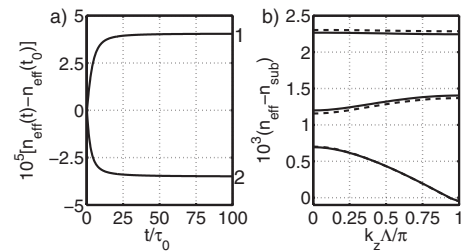


FIG. 15. (a) Simulated changes of the effective refractive index of the mode lying in the first and second band at the edge of the BZ as a function of time. (b) Dashed line: nonlinear band structure corresponding to the steady-state values from part (a), solid line: linear band structure.

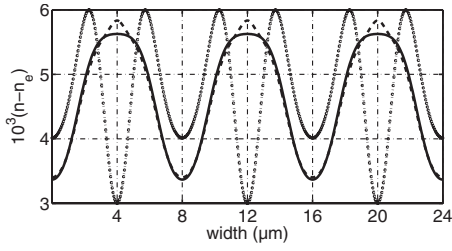


FIG. 16. Modulation of the extraordinary refractive index versus crystal width of the mode located in band two at $k_z = \pi/\Lambda$. Solid line: linear case, dashed line: nonlinear case corresponding to the profile that results in the nonlinear band structure given in Fig. 15(b), dotted line: illustration of the intensity distribution.

served that the profiles of the waveguides becomes more narrow but higher in the nonlinear case. Additionally, the contrast of the modulation is increased, which leads to an increase of the gap between first and second band. At the same time a higher value of the refractive index modulation increases the effective refractive index of the guided modes.

The simulations performed using modes of the second band in the center of the BZ show larger deviations from the experimental data. Figure 17(a) monitors the theoretical curves, and Fig. 7 the experimental results. Contrary to the experiment the calculated effective index changes have high absolute values in the saturation regime. Furthermore, the first band is shifted towards smaller values of the effective index and no zero crossings are found for modes of the second and third band. We want to point out that, when slightly varying the parameters of the (permanent) index profile of the waveguide array, modes of higher bands are strongly affected. Besides the effective refractive indices the amplitudes as well as the ratio of spatial harmonics contributing to the intensity distribution change.

Finally we proceed with the results obtained for excitation of modes of the third band. As in the experimental section we will focus on modes located in the center of the BZ. The amplitudes of the contributing spatial harmonics of the intensity distribution plotted in Fig. 18 show that the first four spatial harmonics have to be considered.

The numerical results plotted in Fig. 19(a) monitor a decrease of the effective refractive index for the mode located

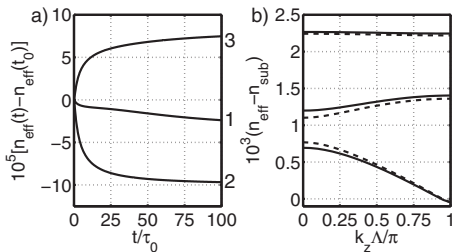


FIG. 17. (a) Time evolution of the effective refractive index changes for the mode of the first, second and third band induced by the intensity distribution of the mode of the second band located in the center of the BZ. Results were obtained utilizing Eq. (9). (b) Solid line: linear band structure, dashed line: nonlinear band structure.

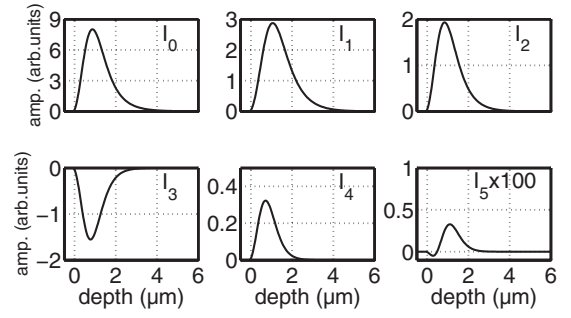


FIG. 18. Amplitudes of the constant component and the first five spatial harmonics of the intensity distribution forming the mode of the third band at $k_z=0$ over crystal depth.

in the third band, whereas modes of the first and second band are shifted to higher values. The corresponding nonlinear band structure in Fig. 19(b) shows a shift of the first and second band towards higher values. Additionally, a reduction of the curvature of second and third bands may be noticed. The modes of the third band in the center of the BZ have smaller values of the effective refractive index in the nonlinear case, when compared with the linear ones. To summarize, the gaps between all neighboring bands have been increased. This agrees well with the experimental observations (see Figs. 8 and 9), although the calculated amplitudes of the induced changes are again slightly smaller.

The explanation of the changes in the band structure can be deduced from Fig. 20. The nonlinear refractive index changes induced by the modes of the third band in the center of the BZ increase the effective width of the channels forming the array. Thus the guiding properties of the waveguides are enhanced. Additionally, the contrast of the modulation is increased because the refractive index is decreased in-between channels.

V. CONCLUSIONS

In conclusion, we have demonstrated that a prism coupling setup allows for measuring the temporal behavior of extended nonlinear FB modes during the build-up of nonlinear index changes. Additionally, the influence of the induced refractive index changes on other modes of the waveguide

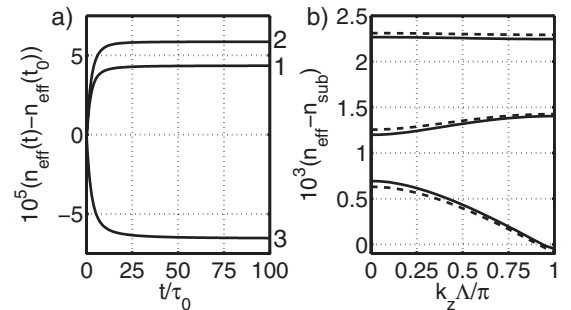


FIG. 19. (a) Simulated changes of the effective refractive index of modes of the first, second, and third band in the center of the BZ as a function of time. (b) Dashed line: nonlinear band structure and solid line: linear band structure.

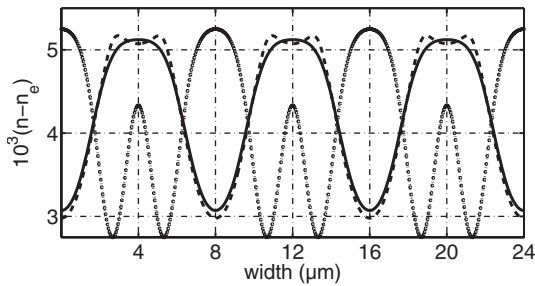


FIG. 20. Modulation of the extraordinary refractive index versus crystal width at the maximum of the intensity distribution (dotted line) of modes located in the third band. The solid line represents the linear case. The dashed line corresponds to the profile of the nonlinear band structure from Fig. 19(b).

array was determined. Experiments were performed using FB modes located in all three guided bands of a waveguide array fabricated by in-diffusion of Ti in Fe-doped LN. To describe the experimental results a simple approach was presented to calculate the band structure of 1D waveguide arrays. Utilizing the one-center band-transport model the temporal build-up of nonlinear index changes induced by the intensity distribution of certain FB modes was described. As in the experiments, the temporal behavior of the effective index changes of the excited mode itself, as well as of modes of other bands at the same value of transverse wave vector, were determined. Finally, for the saturation regime the resulting nonlinear band structures were calculated. As higher spa-

tial harmonics of the induced index changes contribute to the intensity distribution of FB modes, two different approaches were compared. In the first case, spatial harmonics of the intensity distribution that change the refractive index are assumed to be independent from each other, while in the second one, the spatial harmonics mutually influence each other due to a nonlinear mixing term in the current density. The theoretical results, when compared with experimental data, indicate that the latter approach describes the observed changes best. This means that the nonlinear refractive index changes induced by the intensity distribution of extended FB modes exhibit the same characteristics as simultaneously recorded photorefractive gratings. Additionally, our results point to a significant influence of index changes induced by a certain FB mode on the whole band structure. The present study of nonlinear FB modes allows for the detailed investigation of nonlinear mechanisms in LN arrays, such as build-up time constants, saturation values and dark intensity. It also forms the base for the investigation of multiband mixing and nonlinear Zener tunneling, where changes in the band structure induced by the nonlinearity have to be taken into account.

ACKNOWLEDGMENTS

We gratefully acknowledge financial support from the German Federal Ministry of Research (BMBF Grant No. DIP-E6.1) and the Deutsche Forschungsgemeinschaft (DFG Grant No. KI482/8-2).

-
- [1] D. N. Christodoulides, F. Lederer, and Y. Silberberg, *Nature (London)* **424**, 817 (2003).
 - [2] S. Somekh, E. Gamire, A. Yariv, H. L. Garvin, and R. G. Hunsperger, *Appl. Phys. Lett.* **22**, 46 (1973).
 - [3] H. S. Eisenberg, Y. Silberberg, R. Morandotti, A. R. Boyd, and J. S. Aitchison, *Phys. Rev. Lett.* **81**, 3383 (1998).
 - [4] D. N. Christodoulides and R. I. Joseph, *Opt. Lett.* **13**, 794 (1988).
 - [5] T. Pertsch, T. Zentgraf, U. Peschel, A. Bräuer, and F. Lederer, *Phys. Rev. Lett.* **88**, 093901 (2002).
 - [6] H. S. Eisenberg, Y. Silberberg, R. Morandotti, and J. S. Aitchison, *Phys. Rev. Lett.* **85**, 1863 (2000).
 - [7] D. Mandelik, H. S. Eisenberg, Y. Silberberg, R. Morandotti, and J. S. Aitchison, *Phys. Rev. Lett.* **90**, 053902 (2003).
 - [8] R. Morandotti, H. S. Eisenberg, Y. Silberberg, M. Sorel, and J. S. Aitchison, *Phys. Rev. Lett.* **86**, 3296 (2001).
 - [9] J. W. Fleischer, T. Carmon, M. Segev, N. K. Efremidis, and D. N. Christodoulides, *Phys. Rev. Lett.* **90**, 023902 (2003).
 - [10] R. Iwanow, R. Schiek, G. I. Stegeman, T. Pertsch, F. Lederer, Y. Min, and W. Sohler, *Phys. Rev. Lett.* **93**, 113902 (2004).
 - [11] F. Chen, M. Stepić, C. E. Rüter, D. Runde, D. Kip, V. Shandarov, O. Manela, and M. Segev, *Opt. Express* **13**, 4314 (2005).
 - [12] R. Morandotti, U. Peschel, J. S. Aitchison, H. S. Eisenberg, and Y. Silberberg, *Phys. Rev. Lett.* **83**, 4756 (1999).
 - [13] Y. S. Kivshar and M. Peyrard, *Phys. Rev. A* **46**, 3198 (1992).
 - [14] J. Meier, G. I. Stegeman, D. N. Christodoulides, Y. Silberberg, R. Morandotti, H. Yang, G. Salamo, M. Sorel, and J. S. Aitchison, *Phys. Rev. Lett.* **92**, 163902 (2004).
 - [15] M. Stepić, C. Wirth, C. E. Rüter, and D. Kip, *Opt. Express* **31**, 247 (2006).
 - [16] C. E. Rüter, J. Wisniewski, and D. Kip, *Opt. Lett.* **31**, 2768 (2006).
 - [17] D. Kip, *Appl. Phys. B* **67**, 131 (1998).
 - [18] M. Stepić, D. Kip, L. Hadziewicz, and A. Maluckov, *Phys. Rev. E* **69**, 066618 (2004).
 - [19] H. Onodera, I. Awai, and J. I. Ikenoue, *Appl. Opt.* **22**, 1194 (1983).
 - [20] R. L. Holman and P. J. Cressman, *Appl. Phys. Lett.* **38**, 409 (1981).
 - [21] U. Schlarb and K. Betzler, *Phys. Rev. B* **48**, 15613 (1993).
 - [22] J. Rams, A. Tejada, and J. M. Cabrera, *J. Appl. Phys.* **82**, 994 (1997).
 - [23] E. Schneider, P. J. Cressman, and R. L. Holmes, *J. Appl. Phys.* **53**, 4054 (1982).
 - [24] J. Vollmer, J. P. Nisius, P. Hertel, and E. Krätzig, *Appl. Phys. A* **32**, 125 (1983).
 - [25] N. V. Kukhtarev, V. B. Markov, S. G. Odoulov, M. Soskin, and V. L. Vinetskii, *Ferroelectrics* **22**, 949 (1979).
 - [26] V. M. N. Passaro and F. Magno, *Laser Phys.* **17**, 231 (2007).
 - [27] E. M. de Miguel-Sanz, J. Limeres, L. Arizmendi, and M. Carrascosa, *J. Opt. Soc. Am. B* **16**, 1658 (1999).

- [28] H. Lee, *Opt. Lett.* **13**, 874 (1998).
- [29] S. Fries, S. Bauschulte, E. Krätzig, and K. Ringhofer, *Opt. Commun.* **84**, 251 (1991).
- [30] J. Limeres, M. Carrascosa, L. Arizmendi, F. Agulló-López, and P. E. Andersen, *Phys. Rev. B* **65**, 195117 (2002).
- [31] E. Serrano, V. López, M. Carrascosa, and F. Agulló-López, *IEEE J. Quantum Electron.* **30**, 875 (1994).
- [32] M. G. Moharam, T. K. Gaylord, R. Magnusson, and L. Young, *J. Appl. Phys.* **50**, 5642 (1979).
- [33] A. M. Glass, D. von der Linde, and T. J. Negran, *Appl. Phys. Lett.* **25**, 233 (1974).
- [34] A. Yariv, S. S. Orlov, and G. A. Rakuljić, *J. Opt. Soc. Am. B* **13**, 2513 (1996).
- [35] L. Young, M. G. Moharam, E. E. Guibaly, and E. Lun, *J. Appl. Phys.* **50**, 4201 (1979).
- [36] P. Buchhave, *J. Opt. Soc. Am. B* **15**, 1865 (1998).
- [37] J. Limeres, M. Carrascosa, P. M. Petersen, and P. E. Anderson, *J. Appl. Phys.* **88**, 5527 (2000).